© Pol J Radiol 2026; 91: e396-e409
DOI: https://doi.org/10.5114/pjr/222561

Received: 02.03.2026
Accepted: 28.05.2026
Published: 27.08.2026

Polish Journal of Radiology

http://www.polradiol.com

Original paper

Abbreviated MRI protocol in breast cancer diagnosis: comparison with the full diagnostic protocol

Jiameng Si[1,2,A,C,D,E,F,#], Qian Xu[1,2,A,C,D,E,F,#], Xu He[3,A,B,D,F], Fukun Shi[1,2,B,E,F], Yihao Yan[1,2,B,E,F], Junjie Shu[1,2,B,E,F], Zhichao Feng[4,A,D,E], Lan Zhang[1,A,E,F,G]

[1]Department of MRI, the First Affiliated Hospital of Henan University of Chinese Medicine, Zhengzhou, China
[2]First Clinical Medical College of Henan University of Chinese Medicine, Zhengzhou, China
[3]The Second Affiliated Hospital of Wenzhou Medical University, Wenzhou, China
[4]SJTU-Ruijin-UIH Institute for Medical Imaging Technology, Ruijin Hospital, Shanghai Jiao Tong University School of Medicine, Shanghai, China
[#]These authors contributed equally to this study.

Abstract

Purpose: Full diagnostic protocol breast magnetic resonance imaging (FDP-MRI) provides good sensitivity but is constrained by long acquisition times and high costs. Abbreviated magnetic resonance imaging (AMRI) protocols have been proposed to overcome these limitations. This study aimed to develop and validate AMRI protocols and evaluate their diagnostic performance against FDP-MRI in breast cancer diagnosis.

Material and methods: This retrospective study included 220 women (mean age, 51.4 ± 11.3 years) with ultrasonography-detected lesions, who underwent FDP-MRI from September 2021 to September 2024. Three AMRI protocols were derived: non-contrast (NC)-AMRI: T2-weighted imaging + diffusion-weighted imaging (DWI); dynamic contrast-enhanced (DCE)-AMRI A: first post-contrast subtracted (FAST) + maximum-intensity projection (MIP); and DCE-AMRI B: FAST + MIP + DWI. Two radiologists, blinded to pathology, independently interpreted all protocols and classified lesions using the Breast Imaging Reporting and Data System (category ≥ 4 considered positive). Diagnostic performance was compared using Cochran's Q with post-hoc McNemar tests. Receiver operating characteristic curve and areas under the curve (AUCs) were analysed by DeLong's test.

Results: Acquisition times differed significantly between the protocols (FDP-MRI: 16 min 5 s; NC-AMRI: 4 min 20 s; DCE-AMRI A: 2 min 41 s; DCE-AMRI B: 6 min 35 s; all $p < 0.001$). DCE-AMRI A showed the highest sensitivity (85.26%) but the lowest specificity (74.49%). DCE-AMRI B achieved balanced performance with a sensitivity of 83.60% (95% confidence interval, CI: 75.82-89.69) and specificity of 85.71% (95% CI: 77.19-91.96), which was comparable to FDP-MRI (84.42% and 90.81%, respectively; all $p > 0.05$). DCE-AMRI B and FDP-MRI showed equivalent AUCs (0.847 vs. 0.876; $p = 0.085$).

Conclusions: The DCE-AMRI B protocol represents a time-efficient alternative to FDP-MRI, particularly suitable for women with limited tolerance to prolonged prone positioning, offering improved clinical accessibility and workflow efficiency without compromising diagnostic performance.

Key words: breast, abbreviated protocol, full protocol, diagnosis, magnetic resonance imaging.

Introduction

Breast cancer remains a leading cause of female morbidity and mortality worldwide, with increasing incidence and frequently asymptomatic early presentation posing a significant public health challenge [1,2]. Prognosis depends strongly on disease stage at diagnosis, and early

Correspondence address:
Lan Zhang, Department of MRI, the First Affiliated Hospital of Henan University of Chinese Medicine, Renmin Road, Jinshui District, 450000, Zhengzhou, China, e-mail: 13837187787@163.com

Authors' contribution:
A Study design · **B** Data collection · **C** Statistical analysis · **D** Data interpretation · **E** Manuscript preparation · **F** Literature search · **G** Funds collection

This is an Open Access journal, all articles are distributed under the terms of the Creative Commons Attribution-Noncommercial-No Derivatives 4.0 International (CC BY-NC-ND 4.0). License (https://creativecommons.org/licenses/by-nc-nd/4.0/).

detection through systematic imaging can achieve 5-year survival rates of up to 90% [3,4].

Current primary breast imaging modalities include mammography (MG), ultrasonography (US), and magnetic resonance imaging (MRI). While MG offers high specificity (> 90%), its sensitivity (~70%) is notably compromised in women with dense breast tissue; conversely, although US serves as a valuable adjunct, it exhibits suboptimal performance in detecting small invasive carcinomas [5,6]. In contrast, full diagnostic protocol MRI (FDP-MRI) is widely recognised as the most sensitive non-invasive imaging modality for breast cancer detection, particularly for multifocal, multicentric, and occult lesions, providing excellent lesion characterisation without ionising radiation [7,8]. However, its clinical utility is constrained by prolonged acquisition times, complex interpretation, and high costs, which limit accessibility and reduce efficiency [9,10].

To mitigate these limitations, abbreviated MRI (AMRI) protocols retain key diagnostic sequences while substantially reducing scanning and interpretation time [11,12]. In screening settings, AMRI incorporating first post-contrast subtracted (FAST) images and maximum-intensity projection (MIP) has demonstrated diagnostic performance comparable to FDP-MRI [1,13,14]. Diffusion-weighted imaging (DWI) has also shown potential to improve lesion characterisation and specificity [15]. Nevertheless, the optimal composition of AMRI protocols for diagnostic (rather than screening) settings remains uncertain. Previous studies have demonstrated good agreement between AMRI and FDP-MRI in interpreting common abnormalities [16], but they lack systematic, head-to-head comparisons of multiple protocols within the same diagnostic cohort against histopathology [17,18].

Therefore, this study aimed to develop and validate three AMRI protocols derived from FDP-MRI. Through a comparative analysis of their diagnostic performance against FDP-MRI, we sought to identify an optimal protocol that balances high diagnostic accuracy with improved clinical efficiency.

Material and methods

Patients

This study was approved by the Institutional Review Board of the First Affiliated Hospital of Henan University of Chinese Medicine (Approval No. 2022HL-289), and written informed consent was obtained from all participants prior to enrolment.

The clinical and imaging data of female patients with surgically and pathologically confirmed breast lesions were retrospectively analysed between September 2021 and September 2024. All breast MRI examinations were completed before surgical resection and histopathological assessment. Premenopausal women were scheduled to undergo MRI during the mid-cycle phase (days 7-14) of their menstrual period to minimise hormonal influences on background parenchymal enhancement. The inclusion criteria were as follows: (I) Suspicious breast lesions detected on preoperative US, followed by a complete gadopentetate dimeglumine (Gd-DTPA) dynamic contrast-enhanced (DCE)-MRI within two weeks, with the following clinical indications: a) US assessment classified as BI-RADS category 4 or 5 lesions; b) discordance between US findings and clinical palpation; c) suspicious US findings in patients with dense breast tissue; (II) No history of prior local therapy or neoadjuvant chemotherapy before MRI examination; (III) For patients with multiple lesions of different pathological types, only the most poorly differentiated lesion was selected for analysis. The exclusion criteria were as follows: (I) Poor image quality due to severe artifacts; (II) Incomplete clinical data; (III) Presence of regional lymph node or distant metastases; (IV) Pregnancy. Initially, 280 patients who underwent FDP-MRI were enrolled. According to the inclusion and exclusion criteria, 60 patients were excluded. Ultimately, 220 eligible patients were included for statistical analysis (flowchart is shown in Figure 1).

Imaging acquisition

Breast US acquisition

Breast US was performed using a high-frequency colour Doppler ultrasound system (Mindray Resona 8) equipped with a linear-array transducer (9-13 MHz). Patients were positioned supine with both arms elevated overhead to ensure full exposure of the bilateral breasts and axillary regions. Scanning was conducted using the direct contact method with a clockwise radial pattern from the nipple toward the periphery, ensuring continuous coverage with overlapping sections to avoid missed areas. All detected lesions were scanned multidirectionally for comprehensive assessment. The following sonographic features were evaluated on B-mode (grayscale) imaging: (I) Anatomic location and morphology; (II) Maximum lesion diameter; (III) Internal echogenicity and presence of microcalcifications. Colour Doppler imaging was employed to evaluate intralesional vascularity, while spectral Doppler analysis was conducted to quantify flow velocity and resistance index (RI).

Breast MRI acquisition

All MRI examinations were performed on a 3.0T MRI imaging system (Ingenia CX; Philips, Amsterdam, Netherlands) with a 32-channel breast phased-array coil. The FDP-MRI comprised the following sequences: (I) Fast field echo T1-weighted imaging (T1WI); (II) Fat-suppressed T2-weighted imaging (T2WI) with spectral attenuated inversion recovery (SPAIR); (III) DWI with single-shot echo-planar imaging (SS-EPI) at *b*-values

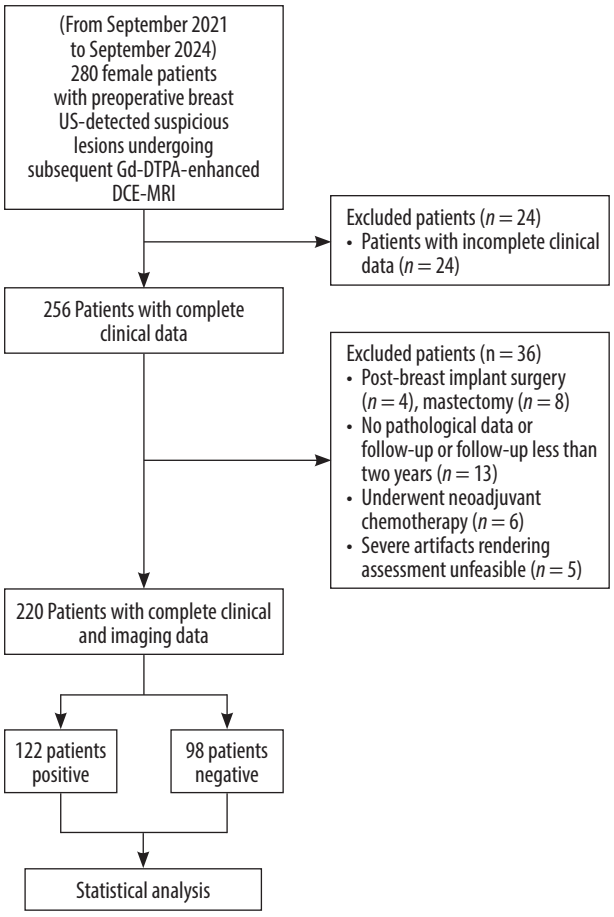

DCE-MRI – dynamic contrast-enhanced magnetic resonance imaging, Gd-DTPA – gadolinium diethylenetriamine pentaacetic acid, US – ultrasonography

Figure 1. Flowchart of study patient collection

of 50 and 800 s/mm², including apparent diffusion coefficient (ADC) mapping; (IV) DCE-T1WI acquired with the mDIXON-FFE sequence. A pre-contrast T1WI mask was obtained prior to intravenous bolus injection of Gd-DTPA at a dose of 0.1 mmol/kg body weight and a flow rate of 2.5 ml/s, followed by a 20 ml saline flush. Six consecutive post-contrast phases were acquired without interval delay, each with a duration of approximately 55 seconds; (V) FAST and MIP images: The pre-contrast T1WI mask and first post-contrast T1WI images were transferred to the Philips IntelliSpace Portal workstation. FAST images were generated by subtracting the pre-contrast from the first post-contrast T1WI. MIP reconstructions were derived from the DCE-MRI dataset to produce three-dimensional projections (MRI parameters are shown in Table 1; FDP-MRI workflow is shown in Figure 2). Three AMRI protocols were extracted from FDP-MRI (Figure 3): (I) Non-contrast AMRI (NC-AMRI), including T2WI + DWI; (II) DCE-AMRI protocol A, including FAST + MIP, (III) DCE-AMRI protocol B, including FAST + MIP + DWI [17,19].

Imaging analysis

Two radiologists (with > 10 and 5 years of experience, respectively) independently reviewed the FDP-MRI and three AMRI protocols. The readers were provided with corresponding US images while remaining blinded to the final pathological results. Any discrepant interpretation was resolved through consensus review. To minimise potential recall bias, a washout period of at least 4 weeks was observed between interpretations of different protocols, with the order of protocol evaluation being randomised [14].

Lesions were classified according to the Breast Imaging Reporting and Data System (BI-RADS) lexicon [20] and the China Anti-Cancer Association breast cancer guidelines [21]. For risk stratification, findings categorised as BI-RADS 1-3 (malignancy probability < 2%) were considered "negative" (not requiring immediate intervention), whereas those categorised as BI-RADS 4-5 (malignancy probability ≥ 2%) were labelled "positive" (warranting biopsy consideration), consistent with clinical management guidelines where BI-RADS 4 lesions warrant biopsy consideration [22,23]. Histopathological findings served as the reference standard for the final diagnosis. In the evaluation of lesions exhibiting diffuse or non-mass enhancement, the entire involved region of abnormal enhancement was treated as a single lesion. In cases of multifocal (multiple lesions within the same quadrant) or multicentric (lesions in different quadrants) disease, if any subregion within this composite area was pathologically confirmed as the same malignant process (e.g. multifocal ductal carcinoma *in situ* [DCIS]), all corresponding imaging findings were assessed collectively. Rigorous correlation between imaging and pathological findings was performed to ensure accurate lesion matching. In breasts with separate

Table 1. Magnetic resonance imaging acquisition parameters

Parameter	T2WI	T1WI	SPAIR	DWI (b = 50,800)	DCE-T1WI mDIXON-FFE)
TR (ms)	3308	505	5636	6275	7.4
TE (ms)	120	8	70	79	1.97
Matrix	312 × 342	312 × 323	280 × 283	132 × 184	280 × 351
Slice thickness (mm)	4.0	4.0	4.0	4.0	2.0
Slice gap (mm)	1.0	1.0	1.0	2.0	–1.0

DCE – dynamic contrast-enhanced, DWI – diffusion-weighted imaging, SPAIR – spectral attenuated inversion recovery sequence, T1WI – T1-weighted imaging, T2WI – T2-weighted imaging, TE – echo time, TR – repetition tim

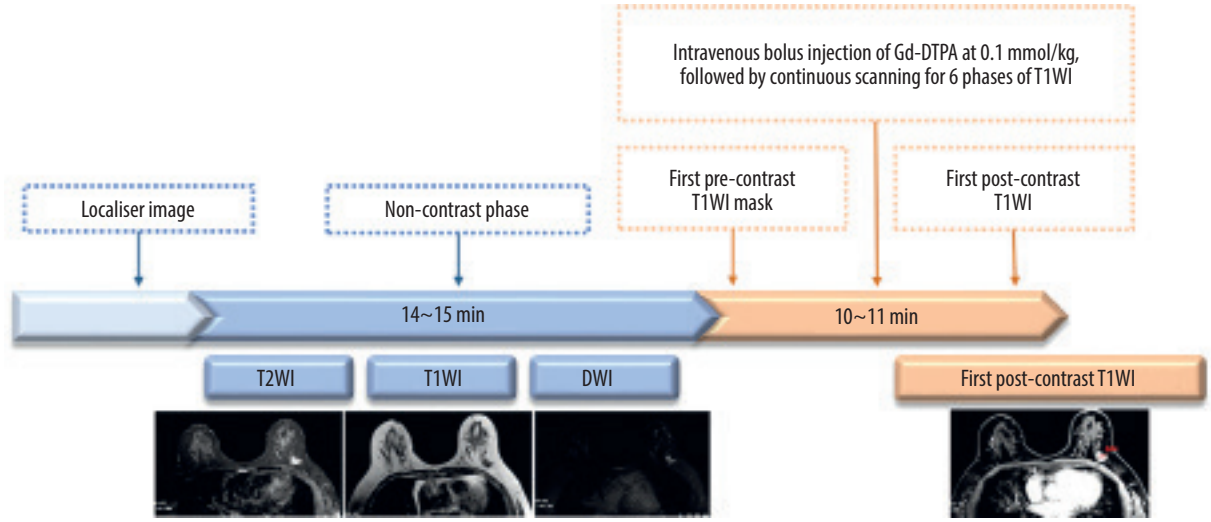

Gd-DTPA – gadolinium diethylenetriamine pentaacetic acid, DWI – diffusion-weighted imaging, T1WI – T1-weighted imaging, T2WI – T2-weighted imaging

Figure 2. FDP-MRI workflow

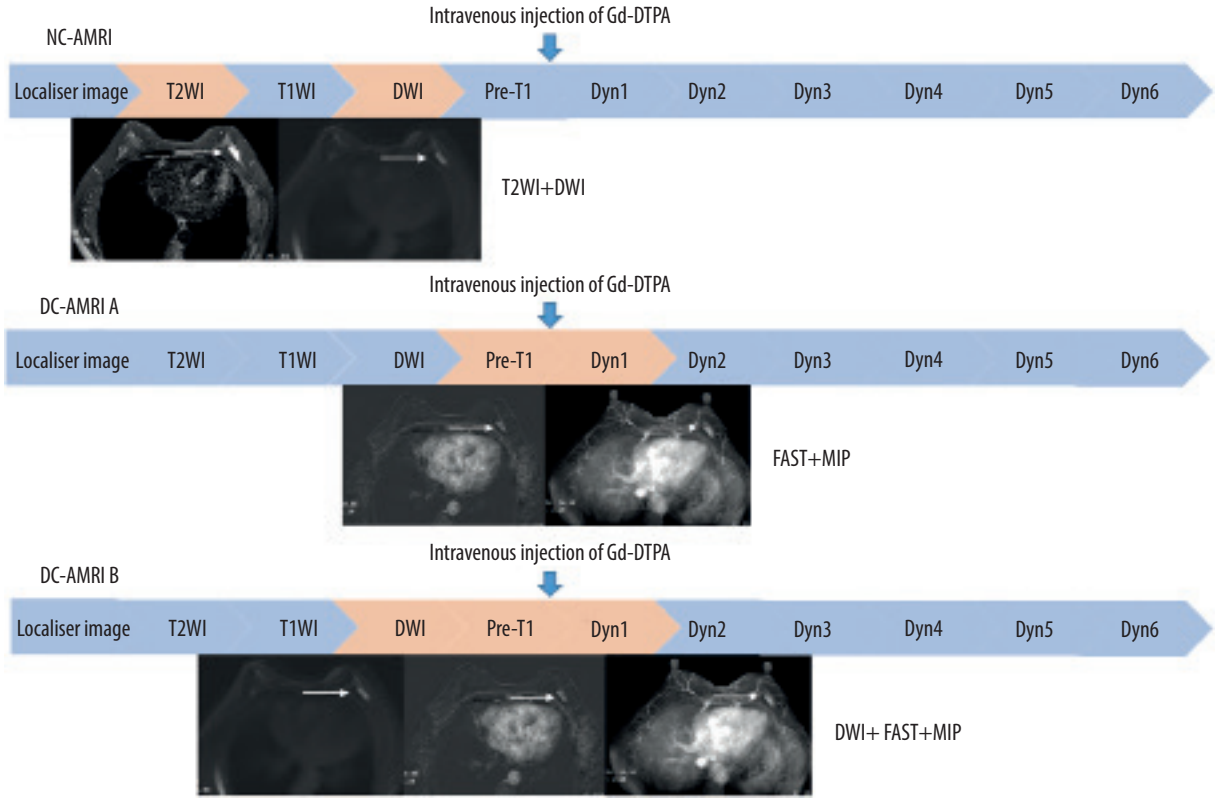

DCE-AMRI – dynamic contrast-enhanced abbreviated MRI, DWI – diffusion-weighted imaging, Dyn – dynamic, Gd-DTPA – gadolinium diethylenetriamine pentaacetic acid, NC-AMRI – non-contrast AMRI, Pre-T1 – pre-contrast T1WI mask, T1WI – T1-weighted imaging, T2WI – T2-weighted imaging

Figure 3. The scheme and example images of three AMRI protocols. The lesions are indicated by arrows

pathological entities, only the most aggressive lesion was included in the analysis.

On ADC maps (b = 800 s/mm²), regions of interest (ROIs) with an area ≥ 0.3 mm² were manually delineated within each lesion, carefully avoiding areas of haemorrhagic foci, cystic components, and adjacent normal glandular tissue. The mean ADC value for each lesion was calculated based on three independent measurements. Receiver operating characteristic (ROC) curve analysis was subsequently performed using these mean ADC values to evaluate diagnostic performance with sensitivity and specificity. Time–intensity curves (TICs) were derived from DCE-MRI data. ROIs were manually drawn on the dynamic phase demonstrating peak lesion enhance-

ment, with exclusion of haemorrhagic/cystic artifacts. Moderate-sized ROIs were selected to ensure representative sampling of contrast-enhancement kinetics while minimising partial volume effects.

The early enhancement ratio (EER), a semi-quantitative metric of initial contrast uptake, was calculated via the following formula:

EER (%) = [(SI post – SI pre)/SI pre] × 100%,

where *SI pre* and *SI post* represent signal intensity before and within 120 seconds after contrast injection, respectively. Lesion enhancement kinetics were categorised into 3 patterns based on EER: slow (EER < 50%), moderate (50% ≤ EER ≤ 100%), and rapid (EER > 100%). Additionally, delayed-phase TIC patterns were classified as persistent, plateau, or washout. Lesion enhancement morphology was categorised as focal, mass-like, or non-mass-like. Background parenchymal enhancement (BPE) was evaluated using standardised semi-quantitative categories: minimal (< 25%), mild (25-50%), moderate (50-75%), or marked (> 75%) enhancement, relative to contralateral normal breast tissue to ensure consistency.

Statistical analysis

All statistical analyses were performed using SPSS 29.0 and MedCalc 20.0.22. Categorical variables are expressed as frequencies and compared using the chi-square (χ^2) test. Normally distributed continuous variables are presented as mean ± standard deviation and compared with the independent-samples *t*-test, with Welch's *t*-test applied for unequal variances. Non-normally distributed continuous variables are summarised as median (interquartile range) and compared using the Wilcoxon test. Inter-observer agreement was assessed with Cohen's kappa coefficient (κ), interpreted as follows: poor (< 0.20), slight (0.20-0.40), fair (0.41-0.60), moderate (0.61-0.80), good (0.81-0.90), and almost perfect (> 0.90). Acquisition times across the four MRI protocols were compared using the Kruskal-Wallis *H* test, followed by post-hoc Mann-Whitney *U* tests with Bonferroni correction. Diagnostic performance including sensitivity, specificity, accuracy, positive predictive value (PPV), and negative predictive value was calculated for each imaging protocol, along with corresponding 95% confidence intervals (CIs). Comparisons among 4 MRI protocols were performed using Cochran's *Q* test, with post-hoc pairwise McNemar's tests with Bonferroni correction. ROC curves were generated, and areas under the curve (AUCs) were compared using the DeLong test. A $p < 0.05$ was considered statistically significant.

Results

Patient characteristics

This study enrolled 220 patients (21-78 years old) with histopathological diagnoses. Among them, 98 benign lesions were identified, including fibroadenoma ($n = 46$), breast adenosis ($n = 38$), intraductal papilloma ($n = 8$), mastitis ($n = 4$), and breast abscess ($n = 2$). Malignant lesions ($n = 122$) included invasive ductal carcinoma ($n = 68$), DCIS ($n = 34$), mucinous adenocarcinoma ($n = 11$), invasive solid papillary carcinoma ($n = 7$), and invasive lobular carcinoma ($n = 7$). Breast density distribution included 141 dense and 79 non-dense cases. Patients with malignant lesions were significantly older than those with benign lesions (51.37 ± 11.33 vs. 44.16 ± 11.08 years; $t = 4.731$, $p < 0.001$). No significant difference was observed in lesion type distribution between the two groups ($\chi^2 = 1.160$, $p > 0.05$).

Significant differences in imaging features were identified between benign and malignant lesions (Table 2). Benign lesions more frequently exhibited slow EER, mild BPE, focal or non-mass enhancement, and persistent-type TIC (all $p < 0.05$). In contrast, malignant lesions were characterised by rapid EER, moderate to marked BPE, mass-like enhancement, and washout-type TIC (all $p < 0.001$). No significant difference was found in lesion margins between the two groups ($p > 0.05$). Using histopathology as the reference standard, the optimal EER cutoff for malignancy discrimination was 111.5%, yielding an AUC of 0.671. At this threshold, the corresponding Youden's index, sensitivity, and specificity were 0.297, 66.40%, and 63.30%, respectively (Figure 4A). Malignant lesions demonstrated significantly lower mean ADC values ($[0.92 \pm 0.23] \times 10^{-3}$ mm²/s) compared to benign lesions ($[1.28 \pm 0.36] \times 10^{-3}$ mm²/s) ($t = 8.945$, $p < 0.001$). ADC values achieved an AUC of 0.809 in differentiating malignant from benign lesions, with an optimal cutoff of 1.061×10^{-3} mm²/s (Youden's index = 0.512), corresponding to a sensitivity of 68.4% and specificity of 82.8% (Figure 4B).

Acquisition times among the four MRI protocols

Acquisition times differed significantly between the four MRI protocols (Kruskal-Wallis $H = 824.380$, $p < 0.001$). All pairwise post-hoc comparisons were significant (all $p < 0.001$). Mean acquisition times were as follows: FDP-MRI, 16 min 5 s; NC-AMRI, 4 min 20 s; DCE-AMRI A, 2 min 41 s; and DCE-AMRI B, 6 min 35 s.

Per-lesion diagnostic performance

Table 3 summarises the diagnostic performance of 5 scanning protocols, and Table 4 shows the pairwise comparisons of the 4 MRI protocols. A significant difference in sensitivity was observed across the protocols (Cochran's $Q = 66.328$, $p < 0.001$). Pairwise comparisons revealed that all 4 MRI protocols outperformed US (58.19%). Specifically, the DCE-AMRI A protocol (85.26%), DCE-AMRI B protocol (83.60%), and FDP-MRI protocol (84.42%) exhibited significantly higher sensitivity than

Table 2. Characteristics of benign and malignant lesions ($n = 220$)

Parameter	Malignant ($n = 122$)	Benign ($n = 98$)	t/χ^2	p-value
Age (years)	51.37 ± 11.33	44.16 ± 11.08	4.731	< 0.001
Menstrual status			21.189	< 0.001
Premenopausal	56 (45.90)	75 (76.53)	21.165	< 0.001
Perimenopausal	16 (13.11)	6 (6.12)	2.952	0.086
Postmenopausal	50 (40.99)	17 (17.35)	13.672	< 0.001
EER				
Slow	7 (5.73)	19 (19.38)	9.716	0.002
Moderate	9 (7.37)	13 (13.26)	2.094	0.148
Rapid	106 (86.90)	67 (67.36)	11.093	0.001
BPE			0.001	0.971
Minimal	28 (22.95)	27 (27.55)	0.613	0.434
Mild	17 (13.93)	41 (41.83)	21.794	< 0.001
Moderate	48 (39.34)	21 (21.42)	8.103	0.004
Marked	29 (23.78)	9 (9.20)	88.020	< 0.001
Enhancement morphology				
Focal	2 (1.63)	18 (18.36)	18.401	< 0.001
Mass-like	89 (72.95)	42 (42.85)	20.431	< 0.001
Non-mass-like	31 (25.42)	38 (38.78)	4.510	0.041
TIC				
Persistent	11 (9.01)	49(50.0)	46.021	< 0.001
Plateau	46 (37.70)	41 (41.83)	0.388	0.580
Washout	65 (53.29)	8 (8.17)	49.891	< 0.001
ADC-value (mm^2/s)	$(0.92 \pm 0.23) \times 10^{-3}$	$(1.28 \pm 0.36) \times 10^{-3}$	7.366	< 0.001

ADC – apparent diffusion coefficient, BPE – background parenchymal enhancement, EER – early enhancement ratio, TIC – time–intensity curve

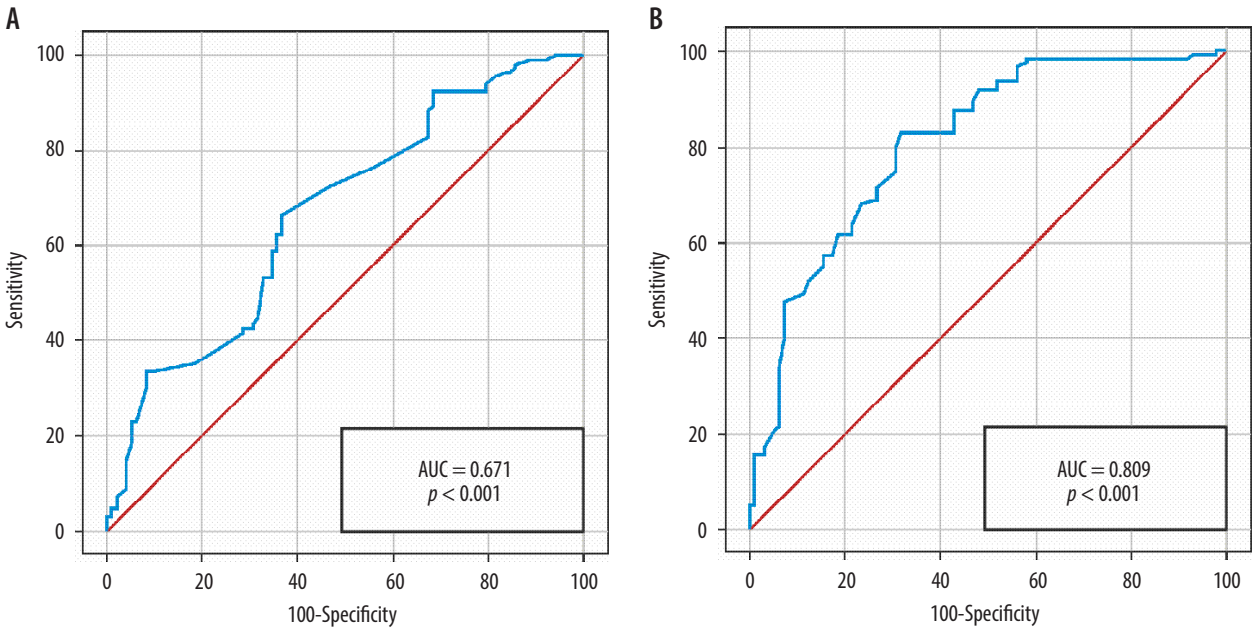

Figure 4. Receiver operating characteristic curves for (**A**) early enhancement ratio and (**B**) apparent diffusion coefficient value in comparing benign and malignant lesions

Table 3. Diagnostic performance among ultrasonography (US) and 4 magnetic resonance imaging (MRI) protocols

Diagnostic performance	Sensitivity (95% CI)	Specificity (95% CI)	Accuracy (95% CI)	PPV (95% CI)	NPV (95% CI)	AUC (95% CI)
US	58.19 (48.92-67.06)	85.71 (77.19-91.96)	70.45 (63.95-76.39)	83.52 (75.32-89.39)	62.22 (56.82-67.33)	0.720 (0.655-0.778)
NC-AMRI	71.42 (62.42-79.33)	87.12 (78.99-92.96)	78.63 (72.62-83.86)	86.73 (79.53-91.66)	72.13 (65.86-83.86)	0.793 (0.733-0.844)
DCE-AMRI A	85.26 (77.68-91.01)	74.49 (64.68-82.76)	80.45 (74.59-85.47)	80.62 (74.63-85.46)	80.22 (72.27-86.31)	0.799 (0.740-0.850)
DCE-AMRI B	83.60 (75.82-89.69)	85.71 (77.19-91.96)	84.54 (79.07-89.05)	87.93 (81.67-92.25)	80.76 (73.61-86.34)	0.847 (0.792-0.892)
FDP-MRI	84.42 (76.42-90.35)	90.81 (83.28-95.71)	87.27 (82.13-91.37)	91.96 (85.93-95.54)	82.40 (75.51-87.67)	0.876 (0.825-0.917)

Data are percentages with numerators/denominators in parentheses and 95% confidence intervals (CI) in brackets.
AMRI – abbreviated MRI, AUC – area under the curve, DCE-AMRI – dynamic contrast-enhanced AMRI, FDP-MRI – full protocol MRI, NC-AMRI – non-contrast AMRI, NPV – negative predictive value, PPV – positive predictive value

Table 4. Pairwise comparisons between the 4 magnetic resonance imaging (MRI) protocols

Group	Sensitivity, *p*-value	Specificity, *p*-value	Accuracy, *p*-value	AUC, *p*-value
NC-AMRI vs. DCE-AMRI A	< 0.001	0.012	0.626	0.874
NC-AMRI vs. DCE-AMRI B	0.003	1.000	0.026	0.025
NC-AMRI vs. FDP-MRI	< 0.001	0.219	< 0.001	< 0.001
DCE-AMRI A vs. DCE-AMRI B	1.000	0.003	0.064	0.018
DCE-AMRI A vs. FDP-MRI	1.000	< 0.001	0.004	< 0.001
DCE-AMRI B vs. FDP-MRI	1.000	0.125	0.180	0.085

AMRI – abbreviated MRI, AUC – area under the curve, DCE-AMRI – dynamic contrast-enhanced AMRI, FDP-MRI – full protocol MRI, NC-AMRI – non-contrast AMRI

NC-AMRI (71.42%) (all $p < 0.05$). As illustrated in Figure 5, a representative case of pathologically confirmed invasive lobular carcinoma was initially classified as BI-RADS 4a on US, suggestive of an inflammatory lesion. MRI demonstrated hyperintensity on T2WI, restricted diffusion with hyperintensity on DWI and corresponding low ADC value (0.536×10^{-3} mm²/s), hyperintensity on MIP, and mild hyperintensity on FAST images. Both FDP-MRI and 3 AMRI protocols correctly classified the lesion as positive.

Significant differences in specificity were observed between the 5 protocols (Cochran's $Q = 43.524$, $p < 0.001$). Pairwise comparisons indicated that the NC-AMRI protocol (87.12%), DCE-AMRI B protocol (85.71%), and FDP-MRI (90.81%) demonstrated significantly higher specificity than the DCE-AMRI A protocol (74.49%) (all $p < 0.05$). As illustrated in Figure 6, a case of pathologically confirmed left breast fibroadenoma was initially rated as BI-RADS 3 on US. MRI revealed mild hyperintensity on T2WI, slight hyperintensity on DWI (ADC value = 1.25×10^{-3} mm²/s), hyperintensity on MIP, and heterogeneous enhancement on FAST. The lesion was correctly classified as negative by the FDP-MRI, NC-AMRI, and DCE-AMRI B protocols, but was misinterpreted as positive by the DCE-AMRI A protocol.

Statistically significant differences in accuracy were observed across US and 4 MRI protocols (Cochran's $Q = 22.540$, $p < 0.001$). Pairwise comparisons revealed that all 4 MRI protocols yielded higher accuracy than US (70.45%), with the FDP-MRI protocol (87.28%) significantly outperforming NC-AMRI (78.63%) (all $p < 0.05$). As illustrated in Figure 7, a case of pathologically confirmed high-grade DCIS was classified as BI-RADS category 4a on US. NC-AMRI interpreted the lesion as negative due to it being isointense on T2WI and the absence of restricted diffusion. However, the lesion demonstrated marked hyperintensity on MIP, non-mass enhancement on FAST, and pronounced enhancement on the first post-contrast T1WI. Both DCE-AMRI protocols and the FDP-MRI correctly identified the lesion as positive.

The AUC of the ROC curve was highest for the FDP-MRI protocol (AUC = 0.876; 95% CI: 0.825-0.917), followed by DCE-AMRI B (AUC = 0.847; 95% CI: 0.792-0.892), DCE-AMRI A (AUC = 0.799; 95% CI: 0.740-0.850), NC-AMRI (AUC = 0.793; 95% CI: 0.733-0.844), and US (AUC = 0.720; 95% CI: 0.655-0.778) (Figure 8). DeLong's test demonstrated that all 4 MRI protocols demonstrated statistically superior performance compared

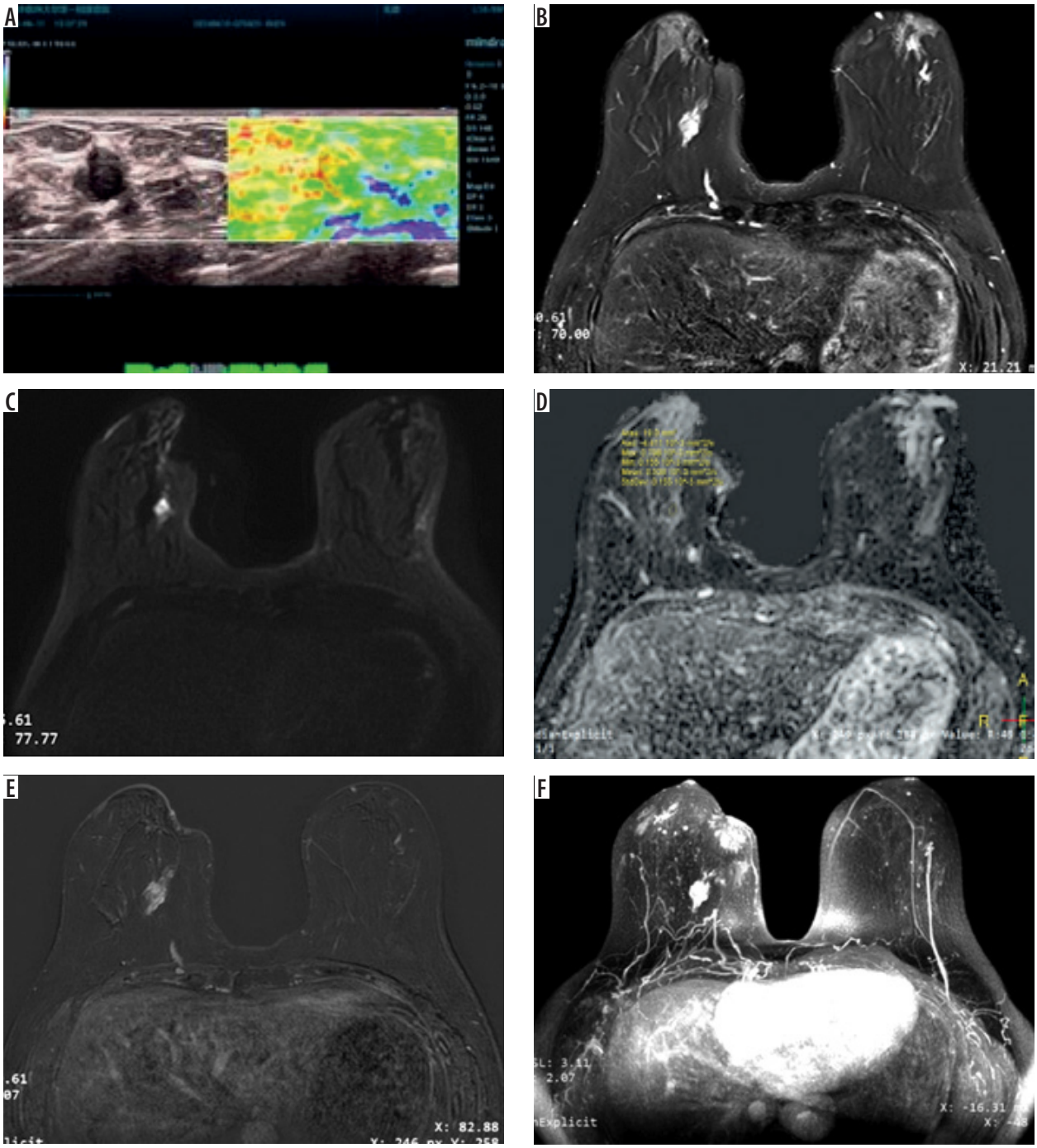

Figure 5. 43-year-old woman with pathologically confirmed invasive lobular carcinoma. Ultrasonography (US) (**A**) shows a hypoechoic nodule (Breast Imaging Reporting and Data System [BI-RADS] 4a). Magnetic resonance imaging (MRI) demonstrates hyperintensity on T2-weighted imaging (T2WI) (**B**), restricted diffusion on diffusion-weighted imaging (DWI) (**C**) with low apparent diffusion coefficient (ADC) (0.536×10^{-3} mm^2/s) (**D**), heterogeneous enhancement on first post-contrast subtracted (FAST) (**E**), and hyperintensity on maximum-intensity projection (MIP) (**F**). All three abbreviated MRI (AMRI) protocols and full diagnostic protocol MRI (FDP-MRI) correctly classified the lesion as positive (BI-RADS ≥ 4). Non-contrast AMRI (NC-AMRI): T2WI + DWI (**B** + **C**); dynamic contrast-enhanced AMRI (DCE-AMRI) A: FAST + MIP (**E** + **F**); DCE-AMRI B: FAST + MIP + DWI (**C** + **E** + **F**)

to US. Furthermore, both the FDP-MRI and DCE-AMRI B protocols exhibited superior diagnostic performance compared to the NC-AMRI and DCE-AMRI A protocols (all $p < 0.05$). No statistically significant difference was found between the FDP-MRI and DCE-AMRI B protocols ($Z = 1.722$, $p > 0.05$).

Interobserver agreement

Interobserver agreement was moderate across all imaging protocols, with κ values as follows: NC-AMRI (κ = 0.791), DCE-AMRI A (κ = 0.793), DCE-AMRI B (κ = 0.782), and FDP-MRI (κ = 0.772).

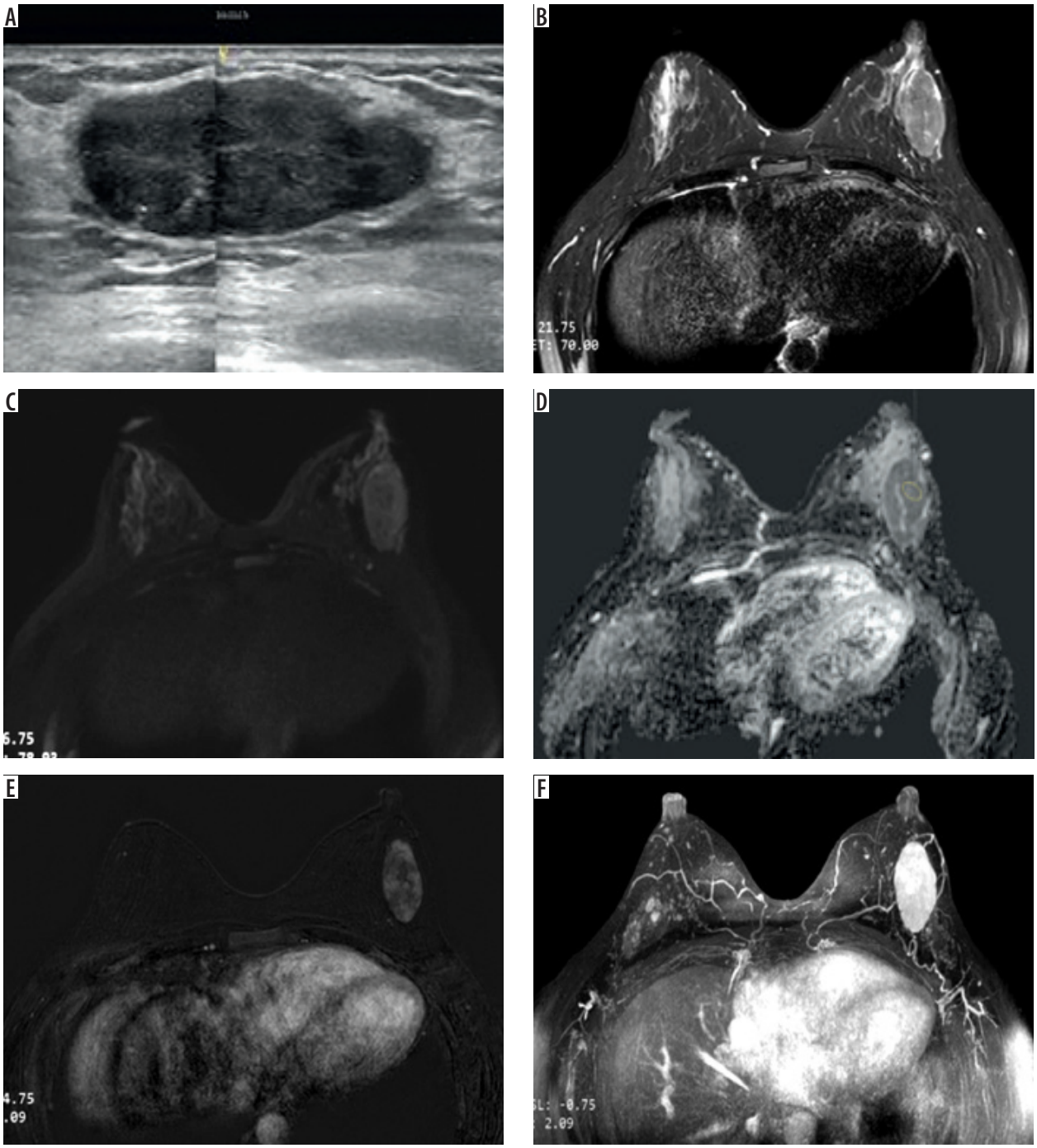

Figure 6. A 44-year-old woman with pathologically confirmed fibroadenoma. Ultrasonography (US) (**A**) shows a hypoechoic nodule (Breast Imaging Reporting and Data System [BI-RADS] 3). Magnetic resonance imaging (MRI) demonstrates mild hyperintensity on T2-weighted imaging (T2WI) (**B**), slight hyperintensity on diffusion-weighted imaging (DWI) (**C**) with apparent diffusion coefficient (ADC) value of 1.25×10^{-3} mm^2/s (**D**), heterogeneous enhancement on first post-contrast subtracted (FAST) (**E**), and hyperintensity on maximum-intensity projection (MIP) (**F**). The lesion was correctly classified as negative (BI-RADS < 4) by full diagnostic protocol MRI (FDP-MRI), non-contrast abbreviated MRI (NC-AMRI), and dynamic contrast-enhanced abbreviated MRI B (DCE-AMRI B), but was misinterpreted as positive by DCE-AMRI A alone. NC-AMRI: T2WI + DWI (**B** + **C**); DCE-AMRI A: FAST + MIP (**E** + **F**); DCE-AMRI B: FAST + MIP + DWI (**C** + **E** + **F**)

Discussion

In this comparative study of three AMRI protocols against FDP-MRI in 220 patients with histopathologically confirmed breast lesions, we made three principal observations. First, all AMRI protocols significantly outperformed US in sensitivity (> 70% vs. 58.19%; $p < 0.001$). Second, the DCE-AMRI B protocol (FAST + MIP + DWI) achieved diagnostic performance comparable to FDP-MRI, with no significant differences in sensitivity, specificity, or AUC, while reducing acquisition time by approximately 60% (from 16 min 5 s to 6 min 35 s). This suggests a viable, time-efficient alternative for breast cancer diagnosis. Third, the DCE-AMRI A protocol (FAST + MIP alone),

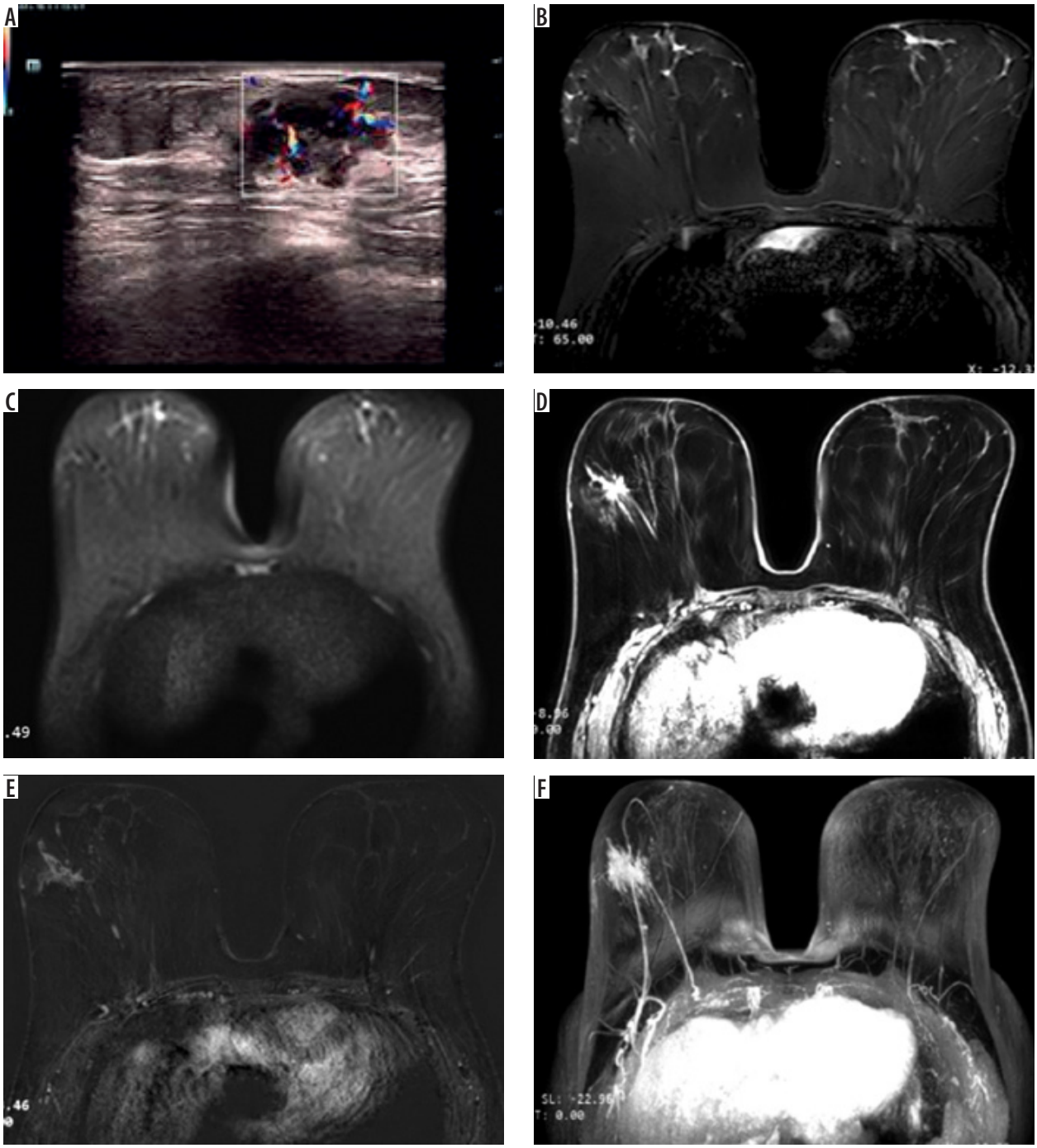

Figure 7. A 64-year-old woman with pathologically confirmed high-grade ductal carcinoma in situ (DCIS). Ultrasonography (US) (**A**) shows a hypoechoic area with arterial flow (Breast Imaging Reporting and Data System [BI-RADS] 4a). Magnetic resonance imaging (MRI) demonstrates the following: isointensity on T2-weighted imaging (T2WI) (**B**), no restricted diffusion on diffusion-weighted imaging (DWI) (**C**), marked enhancement on early post-contrast T1-weighted imaging (T1WI) (**D**), non-mass enhancement on first post-contrast subtracted (FAST) (**E**), and hyperintensity on maximum-intensity projection (MIP) (**F**). The lesion was incorrectly classified as negative by non-contrast abbreviated MRI (NC-AMRI) due to absence of restricted diffusion, but it was correctly identified as positive by both dynamic contrast-enhanced abbreviated MRI (DCE-AMRI) and full diagnostic protocol MRI (FDP-MRI). NC-AMRI: T2WI + DWI (**B** + **C**); DCE-AMRI A: FAST + MIP (**E** + **F**); DCE-AMRI B: FAST + MIP + DWI (**C** + **E** + **F**)

despite having the highest sensitivity (85.26%), demonstrated significantly lower specificity (74.49%) than all other protocols, highlighting the critical role of DWI in reducing false-positive interpretations.

Our findings extend prior work on AMRI validation. Wahab *et al.* [16] demonstrated substantial to excellent intra-reader agreement between AMRI and FDP-MRI in characterising common breast abnormalities (mass, non-mass enhancement, focus), suggesting that subsequent FDP-MRI may not be needed for further characterisation. While their study focused on reader agreement in a small cohort (32 patients) with BI-RADS 0 assessments, our larger cohort (220 patients) with histopathologic validation provides quantitative diagnostic performance metrics

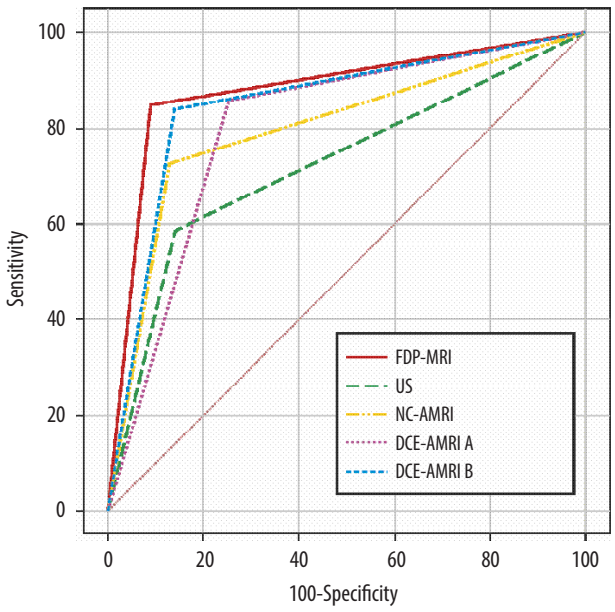

AMRI – abbreviated MRI, DCE-AMRI A – dynamic contrast-enhanced AMRI protocol A, DCE-AMRI B – dynamic contrast-enhanced AMRI protocol B, FDP-MRI – full diagnostic protocol MRI, MRI – magnetic resonance imaging, NC-AMRI – non-contrast AMRI, US – ultrasonography

Figure 8. Receiver operating characteristic curves showing the areas under the curve of five protocols for differentiating benign and malignant breast lesions

that support and refine their conclusion. Notably, the sensitivity of our DCE-AMRI B protocol (83.60%) aligns with the pooled sensitivity of 90% (95% CI: 79-96%) reported in a meta-analysis of AMRI screening studies by Baxter *et al.* [24], and our specificity (85.7%) falls within the range observed across heterogeneous study populations (75-94%) [1,14,25]. This consistency across studies with different designs strengthens the evidence that AMRI can achieve diagnostic performance comparable to FDP-MRI. Furthermore, the invasive cancer detection rate of our DCE-AMRI protocols parallels the incremental cancer detection observed by Comstock *et al.* [25] in the EA1141 trial, where AMRI detected significantly more invasive tumours than digital breast tomosynthesis (11.8 vs. 4.8 per 1000 women), underscoring the robustness of abbreviated approaches even in average-risk populations.

The diagnostic comparability of DCE-AMRI B to FDP-MRI is supported by the complementary strengths of its integrated sequences, which directly address the information needs identified by practicing radiologists. FAST imaging captures early-phase contrast enhancement, critical for distinguishing hypervascular malignancies from background parenchyma while minimising BPE interference [26-28]. MIP facilitates rapid lesion detection and provides an overview of vascular morphology [29,30]. However, as Wahab *et al.* [16] noted, early post-contrast imaging alone may miss subtle areas of persistent or progressive enhancement, which partly explains why 17% of their readers requested delayed-phase sequences. Our incorporation of DWI compensates for this limitation by providing functional information independent of contrast kinetics and BPE, enabling quantitative assessment via ADC values that enhance specificity [31-33]. This proved particularly valuable in diagnostically challenging cases. For instance, in breast abscesses characterised by inflammatory granulation with persistent rim enhancement, DWI identified restricted diffusion within the purulent content to enable confident differentiation from necrotic carcinomas. Similarly, in benign inflammatory lesions such as granulomatous mastitis, which typically present with ill-defined margins on MIP and marked heterogeneous enhancement on FAST, the combination of DWI and TIC analysis helped reduce false-positives and improved diagnostic specificity [34,35].

DCE-AMRI A (FAST + MIP) demonstrated the highest sensitivity (85.26%) among the three protocols, outperforming both FDP-MRI (84.42%) and DCE-AMRI B (83.60%). This superior sensitivity aligns with the finding of Wahab *et al.* [16] that 43% of abnormalities detected only on AMRI (versus FDP-MRI) were identified on early post-contrast imaging. The exceptional capability of FAST + MIP in detecting small, well-differentiated lesions with atypical enhancement patterns, such as sub-5 mm DCIS and invasive cancers, has been well documented [36,37]. However, this sensitivity came at the cost of reduced specificity because reliance solely on enhancement patterns risked misclassifying benign inflammatory lesions. This trade-off mirrors the clinical reality that the "shortest" protocol may not be the "best" protocol, consistent with the observation by Ohlmeyer *et al.* [38] that adding DWI to abbreviated protocols improves specificity without compromising sensitivity. In our cohort, 26% of benign lesions misinterpreted as positive by DCE-AMRI A were correctly reclassified by DCE-AMRI B, underscoring the value of functional imaging in reducing false-positives. This finding also resonates with Lawson *et al.*'s [14] prospective comparison of contrast-enhanced MG, AMRI, and standard FDP-MRI, in which AMRI (comparable to our DCE-AMRI B) achieved high sensitivity but required DWI-like information to maintain specificity in a screening population.

Beyond diagnostic accuracy, the DCE-AMRI B protocol offers significant advantages in terms of patient tolerance and healthcare accessibility. It delivers diagnostic performance comparable to that of FDP-MRI while the acquisition time for DCE-AMRI B protocol (6 min 35 s) is substantially shorter than the time for the FDP-MRI protocol (16 min 5 s). This marked reduction in scan duration directly addresses a key barrier to broader clinical adoption of breast MRI: patient discomfort and claustrophobia. Based on preliminary evidence, patient acceptance revealed that 75% reported a preference for AMRI over MG in a survey of 200 women [39,40], reflecting improved tolerability and confidence in the AMRI protocols. This preference is particularly relevant for patients who struggle with prolonged examinations, such as those with claustrophobia, chronic pain, or mobility limitations.

The shorter scan time of the DCE-AMRI B protocol effectively mitigates these challenges by reducing physical strain and anxiety in the magnet bore, thereby expanding access to a highquality AMRI protocol while maintaining diagnostic accuracy.

Our comparative analysis suggested that while the DCE-AMRI B protocol offers a balanced performance profile suitable for general diagnostic settings, the optimal AMRI protocol may vary depending on specific clinical contexts and priorities. For instance, in a pure screening scenario where maximising sensitivity to avoid missed cancers is paramount, the DCE-AMRI A protocol, despite its lower specificity, might be considered due to its higher sensitivity. Conversely, for problem-solving in cases with ambiguous findings on MG or US, where reducing false positives and improving specificity is critical to avoid unnecessary biopsies, the DCE-AMRI B protocol with DWI provides a clear advantage. Furthermore, for high-risk diagnostic populations or monitoring patients with known lesions, a stratified approach might combine different protocols or selectively add sequences based on individual risk factors and prior imaging findings.

Limitations of the study

This study had several limitations. First, its retrospective design may introduce selection bias, and prospective studies are needed to validate our results. Second, although pathological reviews were blinded, radiologists were aware that all cases were pre-selected by US and pathologically confirmed, potentially introducing interpretation bias. Third, our cohort included a higher proportion of malignant lesions (55.5%) than typically encountered in screening populations, reflecting the diagnostic (rather than screening) setting; this enriched cohort may overestimate PPV and should be considered when generalising to screening contexts. Fourth, the AMRI protocols consisted of only 2-3 sequences, which limited comprehensive BI-RADS feature analysis and restricted outcomes to binary classification (positive or negative). Finally, the single-centre recruitment and modest sample size may affect generalisability; multi-institutional studies with larger cohorts are warranted to confirm the broader applicability. Future multicentre research should further validate whether these protocols enhance key clinical outcomes in high-risk populations, including early detection rates, reduced interval cancers, and minimised false-positive recalls.

Conclusions

The DCE-AMRI B protocol (FAST + MIP + DWI) represents a time-efficient alternative to FDP-MRI, offering comparable diagnostic accuracy with substantially reduced acquisition time. It is particularly suitable for women with limited tolerance for prolonged prone positioning. The DCE-AMRI B protocol stands as a robust, patient-centred tool that maintains high diagnostic performance while improving clinical accessibility and workflow efficiency. Future studies in broader, multi-centre cohorts are warranted to further validate its efficacy and explore its potential for stratified use in clinical scenarios.

Disclosures

1. Institutional review board statement: This study was approved by the Ethics Committee of the First Affiliated Hospital of Henan University of Chinese Medicine (Approval No. 2022HL-289), and written informed consent was obtained from all participants prior to enrolment.
2. Assistance with the article: None.
3. Financial support and sponsorship: None.
4. Conflicts of interest: None.

References

1. Kuhl CK, Schrading S, Strobel K, Schild HH, Hilgers RD, Bieling HB. Abbreviated breast magnetic resonance imaging (MRI): first postcontrast subtracted images and maximum-intensity projection – a novel approach to breast cancer screening with MRI. J Clin Oncol 2014; 32: 2304-2310.
2. Harvey SC, Di Carlo PA, Lee B, Obadina E, Sippo D, Mullen L. An abbreviated protocol for high-risk screening breast MRI saves time and resources. J Am Coll Radiol 2016; 13(11S): R74-R80. DOI: 10.1016/j.jacr.2016.09.031.
3. Deike-Hofmann K, Koenig F, Paech D, Dreher C, Delorme S, Schlemmer HP, Bickelhaupt S. Abbreviated MRI protocols in breast cancer diagnostics. J Magn Reson Imaging 2019; 49: 647-658.
4. Nardin S, Mora E, Varughese FM, D'Avanzo F, Vachanaram AR, Rossi V, et al. Breast cancer survivorship, quality of life, and late toxicities. Front Oncol 2020; 10: 864. DOI: 10.3389/fonc.2020.00864.
5. Rahman WT, Helvie MA. Breast cancer screening in average and high-risk women. Best Pract Res Clin Obstet Gynaecol 2022; 83: 3-14.
6. Farkas AH, Nattinger AB. Breast cancer screening and prevention. Ann Intern Med 2023; 176: ITC161-ITC176. DOI: 10.7326/AITC202311210.
7. Upadhyay N, Wolska J. Imaging the dense breast. J Surg Oncol 2024; 130: 29-35.
8. Cömert D, van Gils CH, Veldhuis WB, Mann RM. Challenges and changes of the breast cancer screening paradigm. J Magn Reson Imaging 2023; 57: 706-726.
9. Leithner D, Moy L, Morris EA, Marino MA, Helbich TH, Pinker K. Abbreviated MRI of the breast: does it provide value? J Magn Reson Imaging 2019; 49: e85-e100. DOI: 10.1002/jmri.26291.

10. Tollens F, Baltzer PAT, Dietzel M, Schnitzer ML, Schwarze V, Kunz WG, et al. Economic potential of abbreviated breast MRI for screening women with dense breast tissue for breast cancer. Eur Radiol 2022; 32: 7409-7419.
11. Ko ES, Morris EA. Abbreviated magnetic resonance imaging for breast cancer screening: concept, early results, and considerations. Korean J Radiol 2019; 20: 533-541.
12. Heacock L, Melsaether AN, Heller SL, Gao Y, Pysarenko KM, Babb JS, et al. Evaluation of a known breast cancer using an abbreviated breast MRI protocol: correlation of imaging characteristics and pathology with lesion detection and conspicuity. Eur J Radiol 2016; 85: 815-823.
13. Mango VL, Morris EA, Dershaw DD, Abramson A, Fry C, Moskowitz CS, et al. Abbreviated protocol for breast MRI: are multiple sequences needed for cancer detection? Eur J Radiol 2015; 84: 65-70.
14. Lawson MB, Partridge SC, Hippe DS, Rahbar H, Lam DL, Lee CI, et al. Comparative performance of contrast-enhanced mammography, abbreviated breast MRI, and standard breast MRI for breast cancer screening. Radiology 2023; 308: e230576. DOI: 10.1148/radiol.230576.
15. Lee S, Choi EJ, Choi H, Byon JH. Comparison of diagnostic performance between classic and modified abbreviated breast MRI and the MRI features affecting their diagnostic performance. Diagnostics (Basel) 2024; 14: 282. DOI: 10.3390/diagnostics14030282.
16. Wahab RA, Albasha H, Martin J, Lee SJ, Zhang B, Brown AL, et al. Characterization of common breast MRI abnormalities: comparison between abbreviated and full MRI protocols. Clin Imaging 2021; 79: 125-132.
17. Drinković M, Drinković I, Milevčić D, Matijević F, Drinković V, Markotić A, et al. Diagnostic and practical value of abbreviated contrast-enhanced magnetic resonance imaging in breast cancer diagnostics. Cancers (Basel) 2022; 14: 5645. DOI: 10.3390/cancers-14225645.
18. Shao Z, Liu P, Zhang S, Lu H. Abbreviated protocol combining quantitative diffusion-weighted imaging: a new strategy increasing diagnostic accuracy for breast magnetic resonance imaging? Gland Surg 2021; 10: 2705-2714.
19. Kataoka M, Honda M. Optimizing an abbreviated MRI protocol for women with dense breasts. Radiology 2025; 315: e250981. DOI: 10.1148/radiol.250981.
20. Eghtedari M, Chong A, Rakow-Penner R, Ojeda-Fournier H. Current status and future of BI-RADS in multimodality imaging, from the AJR special series on radiology reporting and data systems. AJR Am J Roentgenol 2021; 216: 860-873.
21. The Society of Breast Cancer China Anti-Cancer Association, Breast Oncology Group of the Oncology Branch of the Chinese Medical Association. Guidelines for breast cancer diagnosis and treatment by China Anti-cancer Association (2024 edition). China Oncol 2023; 33: 1092-1187.
22. Zhang S, Shao H, Li W, Zhang H, Lin F, Zhang Q, et al. Intra-and peritumoral radiomics for predicting malignant BiRADS category 4 breast lesions on contrast-enhanced spectral mammography: a multicenter study. Eur Radiol 2023; 33: 5411-5422.
23. Interlenghi M, Salvatore C, Magni V, Caldara G, Schiavon E, Cozzi A, et al. A machine learning ensemble based on radiomics to predict BI-RADS category and reduce the biopsy rate of ultrasound-detected suspicious breast masses. Diagnostics (Basel) 2022; 12: 187. DOI: 10.3390/diagnostics12010187.
24. Baxter GC, Selamoglu A, Mackay JW, Bond S, Gray E, Gilbert FJ. A meta-analysis comparing the diagnostic performance of abbreviated MRI and a full diagnostic protocol in breast cancer. Clin Radiol 2021; 76: 154.e23-154.e32. DOI: 10.1016/j.crad.2020.08.036.
25. Comstock CE, Gatsonis C, Newstead GM, Snyder BS, Gareen IF, Bergin JT, et al. Comparison of abbreviated breast MRI vs digital breast tomosynthesis for breast cancer detection among women with dense breasts undergoing screening. JAMA 2020; 323: 746-756.
26. He X, Huang T, Zhang J, et al. Diagnosis of an abbreviated breast MRI protocol based on first post-contrast subtracted for breast cancer. Chinese J Med Imaging 2025; 33: 531-536. DOI: 10.3969/j.issn.1005-5185.
27. Tomida T, Urikura A, Uematsu T, Shirata K, Nakaya Y. Contrast enhancement in breast cancer and background mammary-gland tissue during the super-early phase of dynamic breast magnetic resonance imaging. Acad Radiol 2017; 24: 1380-1386.
28. Kataoka M, Honda M, Sagawa H, Ohashi A, Sakaguchi R, Hashimoto H, et al. Ultrafast dynamic contrast-enhanced MRI of the breast: from theory to practice. J Magn Reson Imaging 2024; 60: 401-416.
29. Morris EA. Rethinking breast cancer screening: ultra FAST breast magnetic resonance imaging. J Clin Oncol 2014; 32: 2281-2283.
30. Vilar VS, Gomes AI, Federicci ÉEF, Ribeiro RLM, Rudner MA, Racy ACS. FAST breast magnetic resonance imaging: a new approach for breast cancer screening? Einstein (Sao Paulo) 2022; 20: eAO0073. DOI: 10.31744/einstein_journal/2022AO0073.
31. Milon A, Flament V, Gueniche Y, Kermarrec E, Chabbert-Buffet N, Darai É, et al. How to optimize breast MRI protocol? The value of combined analysis of ultrafast and diffusion-weighted MRI sequences. Diagn Interv Imaging 2023; 104: 284-291.
32. Amornsiripanitch N, Bickelhaupt S, Shin HJ, Dang M, Rahbar H, Pinker K, Partridge SC. Diffusion-weighted MRI for unenhanced breast cancer screening. Radiology 2019; 293: 504-520.
33. Yan H, Ren W, Jia M, Xue P, Li Z, Zhang S, et al. Breast cancer risk factors and mammographic density among 12518 average-risk women in rural China. BMC Cancer 2023; 23: 952. DOI: 10.1186/s12885-023-11444-7.
34. Alper F, Abbasguliyev H, Özmen S, Yalçin A, Yılmaz Çankaya B, Akçay MN. Clinical, histopathological, imaging, and treatment perspectives of inflammatory granulomatous mastitis: review of the literature. Eurasian J Med 2022; 54 (Suppl 1): S172-S178. DOI: 10.5152/eurasianjmed.2022.22306.
35. Ho, J, Xie YJ, Lin FZ, Yu B. Application of BI-RADS combined with diffusion-weighted imaging and dynamic contrast-enhanced MRI in diagnosis of breast lesions. J Radiat Res Appl Sci 2025; 18: 101726. DOI: 10.1016/j.jrras.2025.101726.
36. Yamaguchi K, Ichinohe K, Iyadomi M, Fujiki K, Yoshinaga Y, Egashira R, Nakazono T. Abbreviated and ultrafast dynamic contrast-enhanced (DCE) MR imaging. Magn Reson Med Sci 2025; 24: 315-331.
37. Kim ES, Cho N, Kim SY, Kwon BR, Yi A, Ha SM, et al. Comparison of abbreviated MRI and full diagnostic MRI in distinguishing

between benign and malignant lesions detected by breast MRI: a multireader study. Korean J Radiol 2021; 22: 297-307.
38. Ohlmeyer S, Laun FB, Bickelhaupt S, Palm T, Janka R, Weiland E, et al. Ultra-high b-value diffusion-weighted imaging-based abbreviated protocols for breast cancer detection. Invest Radiol 2021; 56: 629-636.
39. Kuhl CK. Abbreviated breast MRI: state of the art. Radiology 2024; 310: e221822. DOI: 10.1148/radiol.221822.
40. Son D, Phillips J, Mehta TS, Mehta R, Brook A, Dialani VM. Patient preferences regarding use of contrast-enhanced imaging for breast cancer screening. Acad Radiol. 2022; 29 Suppl 1: S229-S238. DOI: 10.1016/j.acra.2021.03.003.